ACS APPLIED MATERIALS & INTERFACES

Research Article

www.acsami.org

Designed Synthesis of SiO_2/TiO_2 Core/Shell Structure As Light Scattering Material for Highly Efficient Dye-Sensitized Solar Cells

Suim Son, Sun Hye Hwang, Chanhoi Kim, Ju Young Yun, and Jyongsik Jang*

World Class University (WCU) program of Chemical Convergence for Energy & Environment (C_2E_2), School of Chemical and Biological Engineering, Seoul National University, 599 Gwanangno, Gwanakgu, Seoul 151-742, Korea

Supporting Information

ABSTRACT: SiO_2/TiO_2 core/shell nanoparticles (STCS-NPs) with diameters of 110, 240, and 530 nm were fabricated to investigate the influence of the size and refractive index of light-scattering particles on light-scattering properties. The optical properties of STCS-NPs were evaluated and compared with SiO_2−NPs and TiO_2−NPs. The structure of STCS-NPs, consisting of a low refractive index core and high refractive index shell, provides efficient light scattering. The optimized anode film with STCS-NPs had ca. 20% improved power conversion efficiency (PCE).

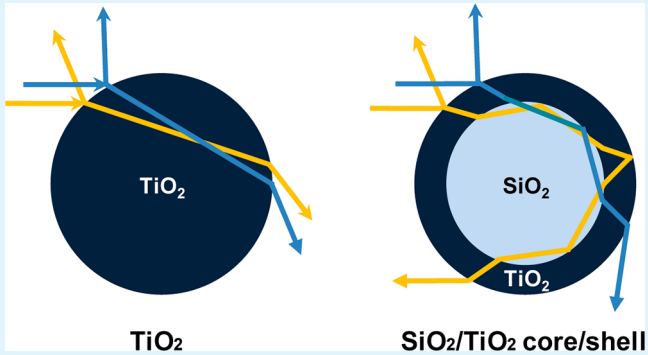

KEYWORDS: *SiO_2/TiO_2 core/shell nanoparticle, light scattering, Mie scattering, dye-sensitized solar cell*

INTRODUCTION

Dye-sensitized solar cells (DSSCs) have attracted tremendous interest in promising candidate for next generation solar cells.[1,2] Up until now, the overall power conversion efficiency (PCE) of DSSCs has reached up to 12%.[3,4] A great deal of effort has been devoted to improving efficiency of DSSCs such as using low-volatility electrolytes, modifying counter-electrode materials, and post-treatment with a $TiCl_4$ precursor.[5] Especially, various approaches have been developed for light harvesting in the working electrode, including increasing the surface area of the metal oxide,[6,7] developing new dyes with broad absorption spectra,[8,9] and introducing light-scattering materials.[10,11]

Light-scattering materials (LSMs) were proposed to improve light absorption in the working electrode. The LSMs are effective in enhancing the light-harvesting capability of the working electrode so as to improve DSSC performance.[12] The light-scattering mechanism consists of two components: optical confinement and increasing the absorption path length. Optical confinement occurs when backscattered light from LSMs becomes trapped in the working electrode. On the other hand, forward-scattered light from LSMs increase the path length in the forward direction. Comparing these two components, optical confinement has a greater effect on enhancing PCE than increasing the path length in the forward direction.[13] On the basis of these optical properties of LSMs, various LSM morphologies have been studied including spheres,[14,15] nanofibers,[16,17] and hollow particles.[18] Also, LSMs with different refractive indices have been investigated such as TiO_2, SiO_2, or Al_2O_3.[12]

Among the LSMs, theoretical studies have been performed to understand the scattering effect of core/shell nanoparticles, because of their wide range of optical manifestations.[19,20] Studies of core/shell structure by several research groups indicated that scattering efficiency depended on the thickness of the shell, the particle size, size distribution, shape, and refractive index. Hsu et al. reported that high scattering efficiency could be achieved using an SiO_2/TiO_2 core/shell particle with optimum diameter of 0.8−1.0 μm and shell thickness of 0.2−0.3 μm.[21] These results were based on theoretical calculations as a function of the particle's optical size and the shell thickness. Small et al. discussed theoretical models that showed improvement in the scattering efficiency for the core/shell structure when the refractive index of the shell material was significantly different than that of surrounding matrix, compared with the core material.[22] However, relatively little attention has been paid to the experimental studies and application of the core/shell structure to DSSCs. It is still challenging to synthesize SiO_2/TiO_2 core/shell structures as LSMs for solar cell applications.

Herein, we report the size-controllable fabrication of SiO_2/TiO_2 core/shell nanoparticles (STCS-NPs) using SiO_2-template sol−gel method. STCS-NPs with 110, 240, and 530 nm size were prepared and the scattering properties of the STCS-NPs were investigated by diffuse reflection spectroscopy (DRS). The optical property of STCS-NP with diameter of 240 (CS240-NP) was compared with that of SiO_2−NPs and TiO_2−NPs, whose diameters are identical to STCS-NPs. Additionally,

Received: February 1, 2013
Accepted: May 1, 2013
Published: May 1, 2013

the photovoltaic properties of the STCS-NPs as scattering materials were evaluated in the working electrode of DSSCs.

Scheme 1 represents a schematic configuration of the assembled DSSC, which is composed of STCS-NPs and

Scheme 1. Schematic Configuration of a Dye-Sensitized Solar Cell (DSSC) That Has SiO_2/TiO_2 Core/Shell Nanoparticles (STCS-NPs) Incorporating Nanocrystalline TiO_2 Particles in the Working Electrode

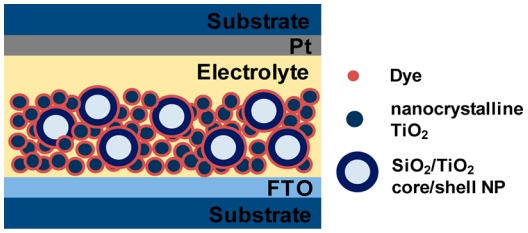

nanocrystalline TiO_2 particles (15–20 nm) in the working electrode. To investigate the dependence of the scattering properties of LSMs on refractive index, we also incorporated SiO_2–NPs and TiO_2–NPs with nanocrystalline TiO_2 particles, respectively.

EXPERIMENTAL SECTION

Preparation of SiO_2, TiO_2, and STCS NPs. Monodisperse SiO_2–NPs 90, 220, 240, and 510 nm in diameter were prepared via seed regrowth method.[23] The sizes of the SiO_2–NPs were controlled by adjusting the amount of TEOS consumed for the formation of the seed ($M_{TEOS,\ seed}$) and TEOS added to the seed dispersion-($M_{TEOS,\ addition}$). The final product was obtained after washing the solution several times with water and drying in a convection oven at 60 °C. TiO_2 nanoparticles were synthesized via sol–-gel reaction. First, 110 mL of absolute ethanol was mixed with 1.5 mL of water. Then, a solution containing 1 mL of titanium isopropoxide (TTIP) and 9 mL of absolute ethanol was dropwised into the 110 mL of absolute ethanol and 1.5 mL of water with vigorous stirring at 298 K for 24 h. The resulting solution was washed several times with water and dried in a vacuum oven at room temperature. The final product was obtained after calcining the powder at 530 °C for 2 h. The prepared SiO_2–NPs with diameter of 90, 220, and 510 nm were used to synthesize STCS-NPs with 10 nm shell thickness. Solution containing 79 mL of ethanol, 3.9 mL of ammonia solution, and 1.4 mL of water was mixed with 1.0 g of SiO_2–NPs in a 100 mL bottle to obtain SiO_2 colloidal solution. Then, 28 mL of acetonitrile was added to the solution with stirring at 4 °C. We used 500 mL bottles for each synthetic reaction. Another solution containing 36 mL of ethanol, 12 mL of acetonitrile, and 1 mL of TTIP was prepared followed by dropwise addition to the colloidal SiO_2 solution. The mixture was vigorously stirred for 12 h. Subsequently, the resulting white solution was dried in oven at 110 °C. After all, 1.5 g of final product was obtained after calcining dried white powder at 600 °C for 6 h.

Assembly of Dye-Sensitized Solar Cell. To prepare a paste with scattering material, we mixed SiO_2, TiO_2, and STCS-NPs with screen-printable TiO_2 nanoparticle paste repectively (Solaronix, Ti-Nanoxide T/sp). The TiO_2 nanoparticle films containing scattering materials were screen-printed on fluorine-doped tin oxide (FTO) glass (15 Ω cm^{-2}, thickness of 2.2 mm) precoated with $TiCl_4$ solution, which was heated at 450 °C for 30 min. The coated films were baked over the same heating profile used previously. For dye adsorption, the resulting TiO_2 films were immersed in anhydrous ethanol containing D719 dye, and kept at room temperature for 24 h. Pt counter electrodes were prepared by dropping 5 mM H_2PtCl_6 solution, followed by heating at 400 °C for 30 min in air. In a sealed cell, iodide-based electrolyte (Idolyte AN-50, Solaronix) was introduced.

Instrument. The morphology of the scattering particles was investigated by transmission electron microscopy (TEM, JEOL JEM-200CX). Field-emission scanning electron microscopy (FE-SEM) and energy-dispersive X-ray spectroscopy (EDX) analysis data were obtained with a JEOL 6700. The scanning TEM/energy-dispersive X-ray (STEM-EDX) line analysis data and EDX analysis data were obtained with a Technai F20 (FEI) spectrometer. Electron energy loss spectroscopy (EELS) mapping of the hybrid nanofibers was performed with a Carl Zeiss LIBRA 200 FE microscope. X-ray diffraction (XRD) data were obtained using an M18XHF-SRA (Mac Science Co.) with a Cu Kα radiation source (λ = 1.5406 Å) at 40 kV and 300 mA (12 kW). Lamda 35 (Perkin-Elmer) provided the spectra of UV–vis diffuse reflectance spectroscopy (DRS) and UV-vis absorption spectroscopy. The cross-section TiO_2 films on the FTO were examined by field-emission scanning electron microscopy (FE-SEM, JEOL 6700). The photocurrent-voltage (I–V) characteristics of the assembled DSSCs were evaluated using a 530 W xenon lamp (XIL model 05A50KS source units). The incident photon-to-current efficiency (IPCE, PV measurements, Inc.) was measured from 300 nm to 800 nm under short-circuit conditions.

RESULTS AND DISCUSSION

To synthesize STCS-NPs, we prepared three different diameters of SiO_2–NPs using modified stöber method. The SiO_2–NPs were coated by TiO_2 shell with sol–gel method, followed by calcining the synthesized STCS-NPs at 600 °C for 6 h. Figure 1 shows transmission electron microscopy (TEM) and field-emission scanning electron microscopy (FE-SEM)

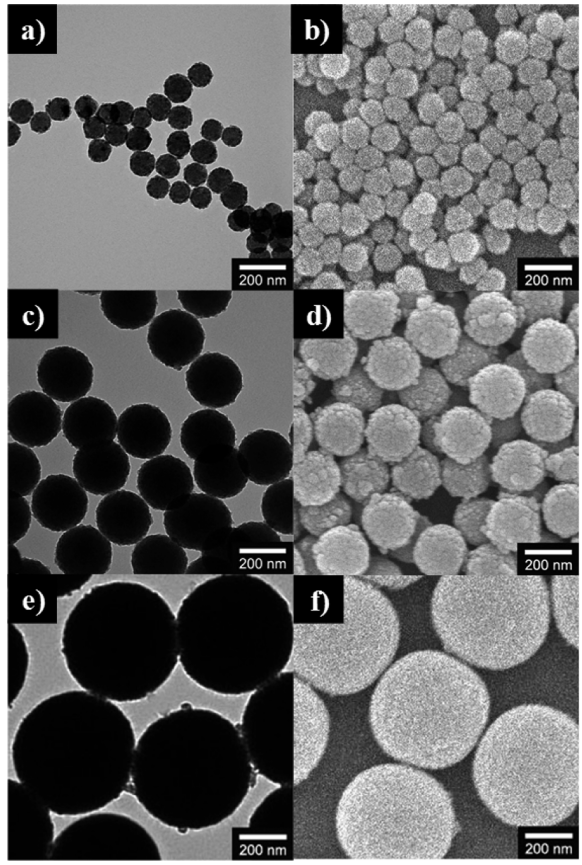

Figure 1. Transmission electron microscopy (TEM) images and field-emission scanning electron microscopy (FE-SEM) images of (a, b) STCS-NPs with diameters of ca. 110 nm, (c, d) STCS-NPs with diameters of ca. 240 nm, (e, f) STCS-NPs with diameters of ca. 530 nm.

images of monodispersed spherical STCS-NPs after calcination at 600 °C. The TiO_2 coated SiO_2−NPs have a fairly uniform diameter of ca. 110, 240, and 530 nm. Their diameters were controlled by varying the size of SiO_2 core template, and the TiO_2 shell thickness was precisely controlled to be uniform (ca. 10 nm). The TEM and SEM images displayed that the SiO_2 core was successfully coated with TiO_2−NPs, resulting in a rough surface morphology.

The atomic ratio between Si and Ti of STCS-NPs was determined by energy dispersive X-ray spectroscopy (EDX) spectra (see the Supporting Information, Figure S1). The results indicated that the atomic ratio between Si and Ti was 46:54 for 110 nm STCS (CS110) NPs, 80:20 for 240 nm STCS (CS240) NPs, and 92:8 for 530 nm STCS (CS530) NPs because of the different sizes of the SiO_2 core. The diameters and shell thicknesses of STCS-NPs were determined by calculating the weight ratio of Si and Ti. The diameters of each STCS-NPs were 110, 240, and 530 nm, and shell thickness was identical at 10 nm.

To determine the atomic distribution, we performed scanning TEM/energy-dispersive X-ray (STEM-EDX) line analyses on STCS-NPs (Figure 2a−c). The Ti line width was

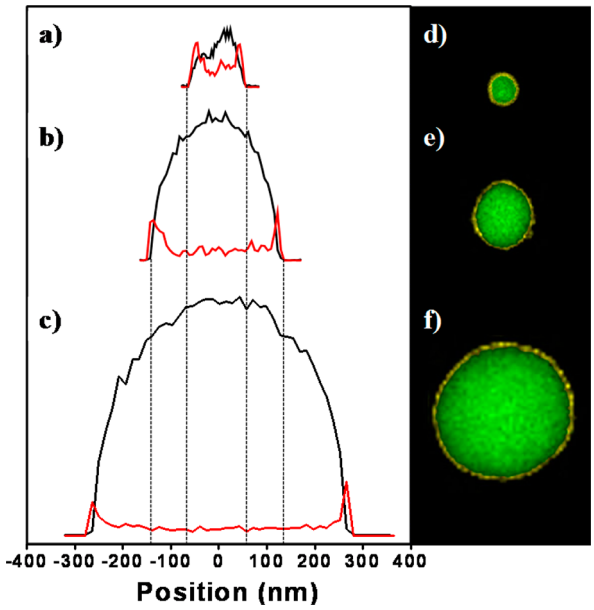

Figure 2. STEM-EDX line mapping and EELS dot mapping of (a, d) STCS-NPs with diameters of ca. 110 nm, (b, e) STCS-NPs with diameters of ca. 240 nm, (c, f) STCS-NPs with diameters of ca. 530 nm.

ca. 10−20 nm and diameters of the NPs were 110, 240, and 530 nm which agreed with the TEM images. This core/shell structure was also confirmed by electron energy loss spectroscopy (EELS) mapping analysis (Figure 2d−f). EELS mapping of the STCS-NPs revealed a distinct division between the SiO_2 core (green: SiO_2) and TiO_2 shell that coated the SiO_2 surface (yellow: TiO_2).

The crystallinity of the STCS-NPs was confirmed by X-ray diffraction (XRD) patterns. Figure S2 in the Supporting Information demonstrates the XRD patterns of STCS NPs; all of the diffraction peaks were perfectly indexed to the anatase phase (JCPDS No. 21-1272). Particularly, the strong diffraction peak at $2\theta = 25.3°$ (101) of the STCS-NPs corresponded well to the peak of anatase TiO_2. It was revealed that electron transport was faster in the anatase phase of TiO_2 than the rutile phase of TiO_2, leading to a better photovoltaic performance.[24] The width of diffraction peaks indicate the crystallinity increasing order of CS110 < CS530 < CS240. Moreover, the diffraction pattern peak intensity of the CS110-NPs was lower than CS240-NPs and CS530-NPs. These results suggested that the TiO_2 shell of CS110-NPs is composed of more irregular polycrystalline. The broad band centered at $2\theta = 22.0°$ implied the existence of SiO_2 amorphous phase (JCPDS No. 29-0085). Judging from these data, the TiO_2 anatase phase coexisted with the SiO_2 amorphous phase in STCS-NPs.

The scattering effect of LSMs is strongly dependent on their diameter and refractive index as Ferber et al. suggested.[25] To investigate the effect of size and refractive index (n) on light-scattering efficiency, the optical reflectance of ∼10 μm thick film of NPs was characterized by UV-Vis diffuse reflectance spectroscopy (DRS). Figure 3a represents the DRS spectra of STCS-NPs with different diameters to evaluate the size dependency of the scattering effect. Comparing the STCS-NPs, the reflectance gets higher with increasing size of NPs. Figure 3b shows the DRS spectra of SiO_2, TiO_2, and STCS-NPs of identical size of 240 nm. To study the effect of refractive index (n) on light scattering efficiency, SiO_2 and TiO_2 NPs were fabricated with identical diameter and morphology of CS240 (see Figure S3 in the Supporting Information). The reflectance of anatase TiO_2−NPs ($n_{TiO2} = 2.49$) was higher than that of SiO_2−NPs ($n_{SiO2} = 1.47$); this was attributed to the increase in the scattering efficiency due to the increase in the refractive index difference between the NPs and the surrounding matrix ($n_{air} = 1.00$). The scattering efficiency of STCS-NPs gets higher than that of SiO_2−NPs because of the presence of high refractive index TiO_2 on SiO_2 core. Compared to TiO_2−NPs, the scattering efficiency of STCS-NPs is lower, which is comparable to the result based on Mie scattering theory.[26]

UV−vis absorption spectra of the 10 μm thick film of dye-adsorbed binary mixtures composed of the LSMs and nanocrystalline TiO_2 particles (TiO_2:LSMs 80:20 wt/wt) was considered to evaluate the scattering effect of the LSMs in the working electrode of DSSCs (Figure 3c, d). Figure 3c displays the absorbance spectra incorporating STCS-NPs with different sizes. The absorbance of the film including CS240-NPs was higher than the film with CS530-NPs. The results indicate that smaller surface area of CS530-NPs because of the larger diameter causes lower dye loading and light absorption. Furthermore, the absorbance of the dye-adsorbed film including CS240-NPs was higher than SiO_2−NPs and TiO_2−NPs as shown in Figure 3d. As mentioned earlier, the surface areas of each particle expected to be comparable due to equivalent diameters of the particles (see Figure S3 in the Supporting Information). Therefore, in the case of the dye-adsorbed binary mixture, the structure of STCS-NPs which composed of low refractive index core and high refractive index shell affects enhanced light absorption efficiency. Especially, the structure of STCS-NPs causes modified light scattering path in the particle and influences high light absorption.

Figure 4 illustrates the light-scattering path of TiO_2 and STCS-NP based on geometric optics.[27] The incident light reflected in a similar manner from the TiO_2−NP and STCS-NP surfaces, because their surfaces consisted of TiO_2. However, for the STCS-NPs, the light refracted in the STCS-NP and went through modified internal reflection path, due to the difference of reflective index in the core/shell structure. Figure 4a

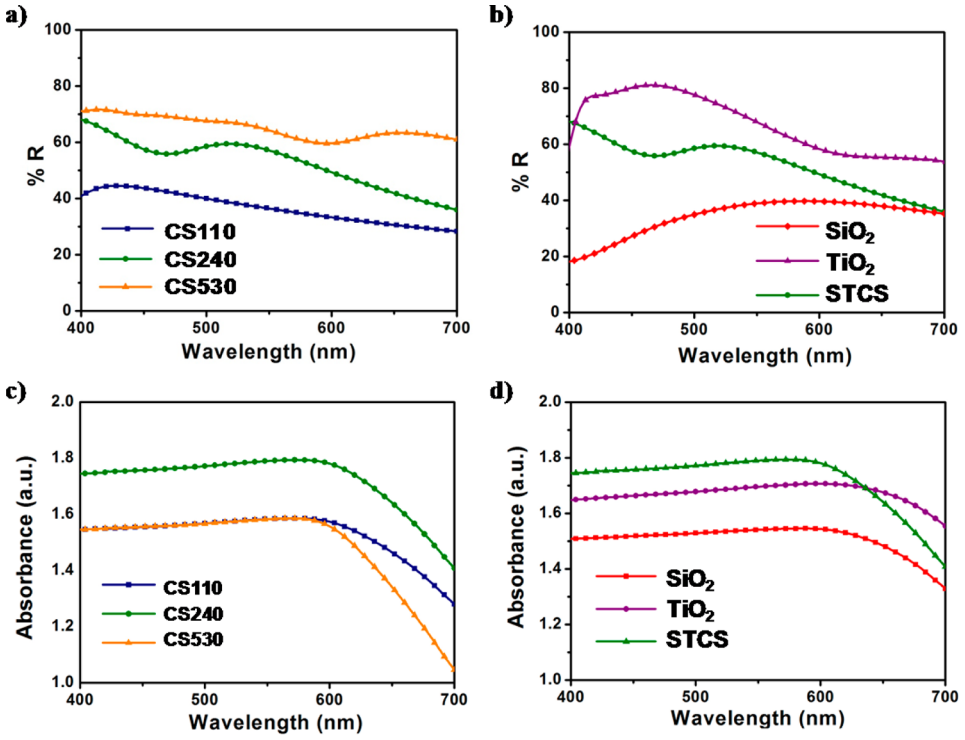

Figure 3. Diffused reflectance spectra (DRS) of (a) STCS-NPs with different diameters, (b) SiO_2, TiO_2, STCS NPs, and UV−vis absorption spectra of (c) STCS-NPs with different diameters, (d) SiO_2, TiO_2, STCS NPs.

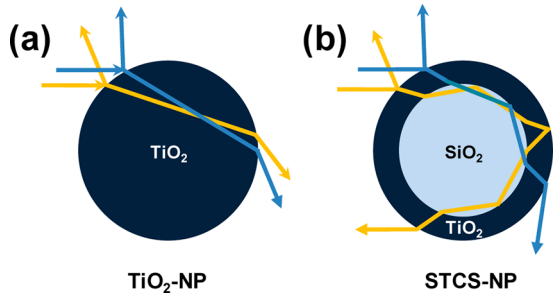

Figure 4. Schematic illustration for light scattering by (a) TiO_2−NP and (b) STCS-NP on the basis of geometric optics.

illustrates the light pathway in a TiO_2−NP. Typically, Mie scattering occurs when the particle size is comparable to the wavelength of incident light; in this case, light is scattered from the large particle in the forward direction, as shown in Figure 4a. Figure 4b displays the modified light pathway in an STCS-NP. In the case of STCS-NPs, it is expected that light undergoes modified internal reflection and mostly emerges from the STCS-NP in the backward direction, resulting in stronger backscattering. This suggests that the structure of the STCS-NP contributed to the increase in the scattering efficiency. In addition, the light scattering of STCS-NPs leads to optical confinement in a DSSC. As mentioned above, the optical confinement has a great effect on enhancing PCE because of the light harvesting effect.[13] Consequently, the PCE should be enhanced because of the increased probability of interaction between the photons and the dye molecules.

To examine the influence of the STCS-NPs on the photovoltaic properties of DSSCs, we incorporated the light-scattering materials (LSMs) such as STCS-NPs, SiO_2−NPs, and TiO_2−NPs with nanocrystalline TiO_2 particles, repectively (TiO_2:LSMs 80:20 wt/wt), which formed a 10-μm-thick film on FTO glass. Figure 5a shows photocurrent density−voltage curves (J−V curves) for the DSSCs with different sizes of STCS-NPs. The photovoltaic parameters, such as the short-

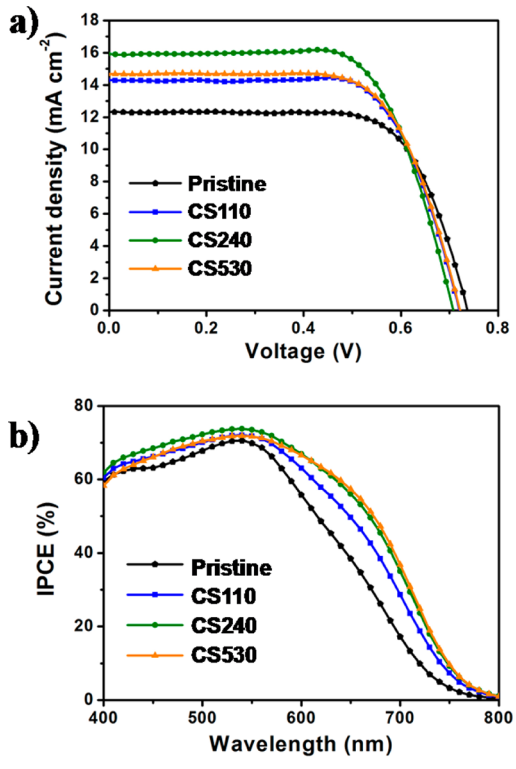

Figure 5. (a) Current density−voltage (J−V) curves and (b) incident photon-to-electron conversion efficiencies (IPCE) of DSSCs based on STCS-NPs with various diameters.

dx.doi.org/10.1021/am400441v | ACS Appl. Mater. Interfaces 2013, 5, 4815−4820

circuit photocurrent density (J_{sc}), open-circuit voltage (V_{oc}), fill factor (FF), and power conversion efficiency (PCE), are summarized in Table 1. By introducing the different sizes of

Table 1. Comparison of Short-Circuit Photocurrent Density (J_{sc}), Open-Circuit Voltage (V_{oc}), Fill Factor (FF), and Power Conversion Efficiency (PCE)

	J_{sc} (mA cm^{-2})	V_{oc} (V)	fill factor	η (%)
pristine	12.4	0.73	0.71	6.5
SiO_2	13.2	0.72	0.72	6.8
TiO_2	14.6	0.73	0.70	7.4
CS110	14.3	0.72	0.71	7.3
CS240	15.9	0.71	0.70	7.9
CS530	14.7	0.72	0.69	7.3

STCS-NPs as LSMs, the solar cell device containing only TiO_2–NPs had a J_{sc} of 12.35 mA cm^{-2} and PCE of 6.49%, whereas the device with CS240-NPs had a J_{sc} of 15.91 mA cm^{-2} and PCE of 7.83%, representing ca. 20% improvement over the film containing only TiO_2–NPs. (Table 1) Interestingly, nevertheless the scattering efficiency of CS530-NPs was highest among the different sizes of STCS-NPs, PCE of CS530-NPs incorporating DSSC was lower than that of CS240 containing DSSC. This result suggests that too large diameter of CS530-NPs causes decrease of internal surface area and insufficient dye attachment.[28] Therefore, the reflectance of the cell containing CS530-NPs might be enhanced but absorbance due to photoexcitaion of the dye was not increased. In the case of J_{sc}, the increase in the J_{sc} for the STCS-NPs was measured following sequence; CS110 < CS530 < CS240. This tendency was well-matched to PCE results. Figure 5b shows the incident-photon-to-current efficiency (IPCE) spectra as a function of wavelength for the DSSCs comprised of the three different sizes of STCS-NPs and pristine DSSC. A noticeable difference on the four types of the samples was observed. Because light scattering efficiency affects to higher IPCE at longer wavelength, the increase of IPCE result at longer wavelength follows the DRS results; CS110 < CS240 < CS530. These results suggest that CS530-NPs have highest scattering effect when apply to DSSC. However, because of lower dye loading of CS530-NPs than that of CS240-NPs, DSSC containing CS240-NPs exhibited highest IPCE at shorter wavelength region (400–600 nm), and the result is well-matched with observed highest J_{sc}.

Figure 6a shows the J–V curves as a function of different LSMs. The photovoltaic parameters are also summarized in Table 1. By incorporating CS240-NPs with nanocrystalline TiO_2, J_{sc} increased significantly from 12.35 mA cm^{-2} (pristine) to 15.91 mA cm^{-2} (STCS). The increase in J_{sc} for the STCS-NPs studied can be summarized as follows: SiO_2 < TiO_2 < STCS; the PCEs followed a similar trend. Our results showed that the DSSC with STCS-NPs had a PCE value of 7.83%, whereas that using TiO_2–NPs achieved a PCE of 7.38%. These results indicate that the PCE of the DSSC with STCS-NPs was 6% improved than that of the device with TiO_2–NPs, because of strong backscattering result from modified light path in the core/shell structure. Finally, DSSCs containing STCS-NPs exhibited an most enhanced PCE of 20%, compared with the pristine DSSC containing only nanocrystalline TiO_2 particles whose PCE value was 6.49%. The results suggest that the optical confinement effect of scattered light from STCS-NPs improved the PCE of the cell. Figure 6b shows the IPCE

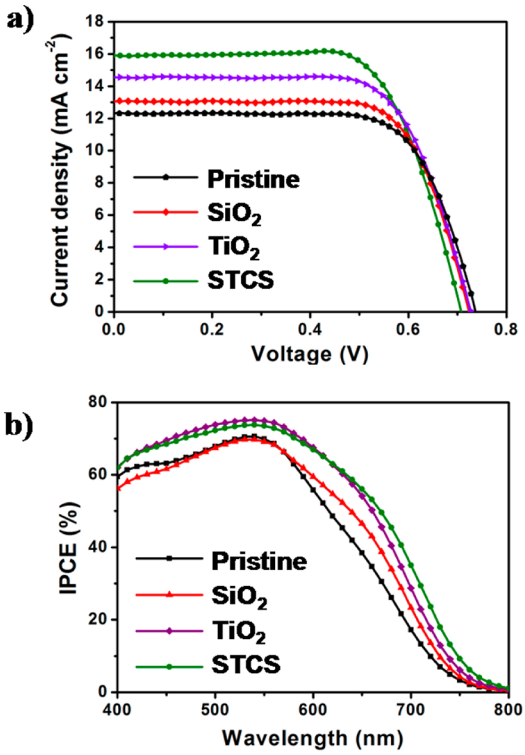

Figure 6. (a) Current density–voltage (J–V) curves and (b) incident photon-to-electron conversion efficiencies (IPCE) of DSSCs based on SiO_2–NPs, TiO_2–NPs, and STCS-NPs as light scattering materials.

spectra as a function of wavelength for the four samples. The absolute IPCE of STCS was the highest over the longer wavelength range, which is in good agreement with the observed highest J_{sc}.

In conclusion, we fabricated monodisperse SiO_2/TiO_2 core/shell nanoparticles (STCS-NPs) with diameters of 110, 240, and 530 nm to investigate the effect of size and refractive index on light-scattering properties. Uniform shell thickness was ca. 10 nm and the crystallinity of the TiO_2 shell was revealed to anatase phase. The light scattering efficiency was increased with increasing size of NPs. However, STCS-NPs with diameter of 530 nm incorporating TiO_2–NPs shows lower efficiency than 240 nm due to insufficient dye adsorption. Also, it was shown that the structure of the STCS-NPs, consisting of a low refractive index core and high refractive index shell, induced optical confinement in a working electrode, thus contributed to the strong scattering efficiency. Additionally, for the same particle size and film thickness, the DSSC incorporating STCS-NPs exhibited the most enhanced PCE, compared with that using SiO_2 and TiO_2 NPs. Accordingly, the power conversion efficiency of CS240-NPs was improved by up to 7.9%, higher than those of conventional working electrode made of nanocrystalline TiO_2–NPs. Finally, the designed synthesis of scattering materials considering refractive indices could provide interesting new opportunities for the development of highly efficient DSSCs.

■ ASSOCIATED CONTENT

Ⓢ Supporting Information

EDX spectra, XRD patterns, and TEM images of STCS-NPs. This material is available free of charge via the Internet at http://pubs.acs.org/.

AUTHOR INFORMATION

Corresponding Author
*E-mail: jsjang@plaza.snu.ac.kr.

Notes
The authors declare no competing financial interest.

ACKNOWLEDGMENTS

This work was supported by Global Frontier R&D Program on Center for Multiscale Energy System funded by the National Research Foundation under the Ministry of Education, Science and Technology, Korea(2011-0031573) and WCU (World Class University) program through the National Research Foundation of Korea funded by the Ministry of Education, Science and Technology (R31-10013).

REFERENCES

(1) O'Regan, B.; Grätzel, M. *Nature* **1991**, *353*, 737−740.
(2) Grätzel, M. *Nature* **2001**, *414*, 338−344.
(3) Yella, A.; Lee, H. W.; Tsao, H. N.; Yi, C.; Chandiran, A. K.; Nazeeruddin, M. K.; Diau, E. W. G.; Yeh, C. Y.; Zakeeruddin, S. M.; Grätzel, M. *Science* **2011**, *334*, 629−634.
(4) Hagfeldt, A.; Boschloo, G.; Sun, L.; Kloo, L.; Pettersson, H. *Chem. Rev.* **2010**, *110*, 6595−6663.
(5) Cho, S.; Hwang, S. H.; Kim, C.; Jang, J. *J. Mater. Chem.* **2012**, *22*, 12164−12171.
(6) Agarwala, S.; Kevin, M.; Wong, A. S. W.; Peh, C. K. N.; Thavasi, V.; Ho, G. W. *ACS Appl. Mater. Interfaces* **2010**, *2*, 1844−1850.
(7) Chen, D.; Huang, F.; Cheng, Y. B.; Caruso, R. A. *Adv. Mater.* **2009**, *21*, 2206−2210.
(8) Hara, K.; Kurashige, M.; Dan-Oh, Y.; Kasada, C.; Shinpo, A.; Suga, S.; Sayama, K.; Arakawa, H. *New J. Chem.* **2003**, *27*, 783−785.
(9) Robertson, N. *Angew. Chem., Int. Ed.* **2006**, *45*, 2338−2345.
(10) Zheng, Y. Z.; Tao, X.; Hou, Q.; Wang, D. T.; Zhou, W. L.; Chen, J. F. *Chem. Mater.* **2011**, *23*, 3−5.
(11) Hwang, S. H.; Kim, C.; Song, H.; Son, S.; Jang, J. *ACS Appl. Mater. Interfaces* **2012**, *4*, 5287−5292.
(12) Zhang, Q.; Dandeneau, C. S.; Zhou, X.; Cao, C. *Adv. Mater.* **2009**, *21*, 4087−4108.
(13) Usami, A. *Sol. Energy Mater. Sol. Cells* **2000**, *64*, 73−83.
(14) Yu, I. G.; Kim, Y. J.; Kim, H. J.; Lee, C.; Lee, W. I. *J. Mater. Chem.* **2011**, *21*, 532−538.
(15) Huang, F.; Chen, D.; Zhang, X. L.; Caruso, R. A.; Cheng, Y. B. *Adv. Funct. Mater.* **2010**, *20*, 1301−1305.
(16) Yang, L.; Leung, W. W. F. *Adv. Mater.* **2011**, *23*, 4559−4562.
(17) Yu, K.; Chen, J. *Nanoscale Res. Lett.* **2009**, *4*, 1−10.
(18) Koo, H. J.; Kim, Y. J.; Lee, Y. H.; Lee, W. I.; Kim, K.; Park, N. G. *Adv. Mater.* **2008**, *20*, 195−199.
(19) Aden, A. L.; Kerker, M. *J. Appl. Phys.* **1951**, *22*, 1242−1246.
(20) Johnson, R. W.; Thiele, E. S.; French, R. H. *Tappi J.* **1997**, *80*, 233−239.
(21) Hsu, W. P.; Yu, R.; Matijević, E. *J. Colloid Interface Sci.* **1993**, *156*, 56−65.
(22) Small, A.; Hong, S.; Pine, D. *J. Polym. Sci., Part B: Polym. Phys.* **2005**, *43*, 3534−3548.
(23) Watanabe, R.; Yokoi, T.; Kobayashi, E.; Otsuka, Y.; Shimojima, A.; Okubo, T.; Tatsumi, T. *J. Colloid Interface Sci.* **2011**, *360*, 1−7.
(24) Shankar, K.; Mor, G. K.; Prakasam, H. E.; Varghese, O. K.; Grimes, C. A. *Langmuir* **2007**, *23*, 12445−12449.
(25) Ferber, J.; Luther, J. *Sol. Energy Mater. Sol. Cells* **1998**, *54*, 265−275.
(26) Johnson, R. W.; Thiele, E. S.; French, R. H. *Tappi J.* **1997**, *80*, 233−239.
(27) Takano, Y.; Liou, K. N. *Appl. Opt.* **2010**, *49*, 3990−3996.
(28) Geng, Y. L.; Qiu, C. W.; Zouhdi, S. *J. Appl. Phys.* **2008**, *104*, 034909-1−034909-10.